Journal of *Xenobiotics*

MDPI

Article

Fungal Transformation and Oxalate-Mediated Mineralization of Heavy Metal Oxides by *Aspergillus aculeatus*

Thanakorn Sawangchart [1], Sutee Chutipaijit [2], Bunyarit Meksiriporn [3], Worapat Narueban [3], Worrathon Tilokkarn [4], Pattareewan Imsuwan [5] and Thanawat Sutjaritvorakul [1,5,*]

[1] Department of Petrochemicals and Environmental Management, Faculty of Engineering, Pathumwan Institute of Technology, Bangkok 10330, Thailand; sawangchart@hotmail.com
[2] School of Integrated Innovative Technology, King Mongkut's Institute of Technology Ladkrabang, Bangkok 10520, Thailand; sutee.ch@kmitl.ac.th
[3] Department of Biology, School of Science, King Mongkut's Institute of Technology Ladkrabang, Bangkok 10520, Thailand; bunyarit.me@kmitl.ac.th (B.M.); 65050785@kmitl.ac.th (W.N.)
[4] Department of Industrial Engineering, Faculty of Engineering, Pathumwan Institute of Technology, Bangkok 10330, Thailand; vorrathon.ti@pit.ac.th
[5] Faculty of Science and Technology, Pathumwan Institute of Technology, Bangkok 10330, Thailand; pattareewan.im@gmail.com
* Correspondence: thana5306@hotmail.com or thanawat@pit.ac.th

Abstract

Fungal transformation is increasingly recognized as an important process influencing metal solubilization and immobilization in soil environments. In this study, a fungal strain (PTW4) isolated from mining-contaminated soil was molecularly identified as *Aspergillus aculeatus*. The strain was evaluated for its ability to solubilize and transform several heavy metal oxides, including ZnO, Pb_3O_4, Cu_2O, and MoO_3. PTW4 produced consistent halo formation across all tested oxides, accompanied by progressive acidification of the culture medium, suggesting organic acid-mediated solubilization. Characterization of extracellular precipitates by SEM-EDS and XRD indicated mineral phases consistent with oxalate-associated biominerals, including zinc oxalate dihydrate ($ZnC_2O_4 \cdot 2H_2O$), lead oxalate (PbC_2O_4), and copper oxalate hydrate ($CuC_2O_4 \cdot xH_2O$). These minerals represent low-solubility phases that may reduce metal mobility in the surrounding environment. In contrast, molybdenum did not precipitate under the experimental conditions, suggesting metal-specific constraints in fungal biomineralization processes. Although organic acid production was not directly quantified, identification of oxalate mineral phases supports an oxalate-associated mineralization mechanism. Overall, the results provide evidence for heavy metal solubilization and selective extracellular precipitation consistent with oxalate biomineral formation by *A. aculeatus* PTW4, highlighting its potential relevance to fungal-mediated bioremediation and selective bioleaching processes.

Keywords: bioremediation; heavy metals; fungal biomineralization; metal solubilization; oxalate-mediated immobilization

Check for updates

Academic Editor: Nikolaos Labrou

Received: 19 January 2026
Revised: 20 February 2026
Accepted: 27 February 2026
Published: 1 March 2026

Copyright: © 2026 by the authors. Licensee MDPI, Basel, Switzerland. This article is an open access article distributed under the terms and conditions of the Creative Commons Attribution (CC BY) license.

1. Introduction

Many industries have employed various heavy metal compounds in their operations, in particular mining, electronics, petrochemicals, semiconductors, and iron and steel production. The use of heavy metal compounds has substantially increased with industrial expansion and economic development. This leads to issues of heavy metal contamination in the environment, which can contaminate the food chain and ultimately affect human

health [1,2]. Heavy metal oxides are compounds generated by the reaction between heavy metals and oxygen. They are of great interest due to their unique properties and applications in various fields, including catalysts, agricultural pesticides, paints, cosmetics, ceramics, and engineered nanomaterials [3,4]. Although most metal oxides are not biologically available due to their insolubility in water, they may also exhibit an effect on the environment and human health [4]. Chemical and physical methods, including membrane separation, ion exchange, redox reaction, chemical precipitation, and evaporation, have been developed to remove heavy metal compounds from the contaminated site. These techniques are highly efficient, but they have some limitations, such as extreme conditions, energy consumption, and cost [4,5].

To address the limitations associated with chemical and physical methods, biological methods have attracted considerable interest due to their environmentally friendly nature and low cost. Bioremediation refers to the use of living organisms, including plants, microalgae, bacteria, and fungi, to degrade, transform, or detoxify environmental pollutants into less harmful forms. It has become an increasingly important approach for the treatment of hazardous organic and metal contaminants. While some organic pollutants can serve as carbon or energy sources for microorganisms, metals cannot be metabolized in this manner and are instead transformed through processes such as solubilization, complexation, and biomineralization. In the context of metal-contaminated environments, fungal-mediated biotransformation has emerged as an effective mechanism for altering metal mobility and speciation [5–7].

Fungi are chemoheterotrophic microorganisms which are commonly found in natural environments, including in polluted areas. Their major role as decomposers in ecosystems also plays a vital role in the leaching and weathering of mineral rocks, and are related to transformation of heavy metal compounds [8]. Moreover, they can produce a wide variety of metabolites which is crucial to the bioremediation process [9,10]. Fungi interact with heavy metal transformation processes in several ways, through processes of accumulation, solubilization, and immobilization, which renders them the capacity to tolerate and detoxify heavy metal compounds [11]. In the solubilization process, many fungi solubilize metal ions from mineral rocks or insoluble compounds to increase metal bioavailability, while in the immobilization process, metal ion bioavailability will be reduced by extracellular precipitation in the form of metal complex crystals. Both primary and secondary metabolites generated by fungi are involved in metal transformation, such as amino acids, organic acids, and phenolic compounds. These metabolites are essential to the chemical reaction on the metal compounds [12]. However, the ability to tolerate heavy metal toxicity is also important. Many reports revealed that fungi isolated from contaminated sites exhibit a remarkable ability to tolerate high concentrations of heavy metals and other pollutants [13–16]. They demonstrated the encouraging potential for bioremediation of fungal species isolated from polluted locations.

Fungal-mediated transformation processes of heavy metals, including solubilization and immobilization, are central to understanding how fungi influence metal behavior at the microscale. It was hypothesized that fungi isolated from mining-contaminated soils would exhibit enhanced metal solubilization capacity and potentially facilitate selective extracellular precipitation of metals as oxalate-associated biominerals. Therefore, this study aimed to investigate the transformation of heavy metal oxides by soil-derived fungal isolates from mining-contaminated sites in Thailand, with particular emphasis on solubilization and extracellular mineralization processes.

2. Materials and Methods

2.1. Fungal Isolation, Identification and Maintenance

Polluted soil was collected from a contaminated area in a mine in Phichit province, Thailand. Surface soil (0–15 cm depth) was collected from multiple points within the contaminated area and composited prior to fungal isolation. The soil was characterized as sandy loam with an initial pH of 6.7. The site has a history of mining activities associated with metal contamination. The soil sample was kept in sterile polythene bags, and stored in a portable cooler for further study. The serial dilution method was used for the fungal isolation under sterile conditions, and the detail was described based on the method of Li et al. [17]. The obtained fungal isolates were purified into the pure cultures. Each pure culture was inoculated and maintained on potato dextrose agar (PDA) at room temperature (25 °C). Fungi were preliminarily identified according to their morphological structures by using the lactophenol cotton blue (LPCB) dropped slide mounts and observed under a light microscope (Olympus, CX23, Olympus Corporation, Tokyo, Japan) [18]. They were classified following Barnett and Hunter [19]. For the selected strain, the identification was confirmed by molecular genetic techniques. Fungal DNA was extracted from fresh mycelia using a standard fungal DNA extraction protocol. The internal transcribed spacer (ITS) region was amplified using primers ITS1 and ITS4. PCR reactions were performed in a total volume of 25 µL containing 1 × PCR buffer (Thermo Fisher Scientific, Waltham, MA, USA), 2.0 mM $MgCl_2$, 0.2 mM of each dNTP, 0.4 µM of each primer, 1 U Taq DNA polymerase, and approximately 20–50 ng of template DNA. The PCR cycling conditions were as follows: initial denaturation at 95 °C for 5 min; followed by 35 cycles of denaturation at 95 °C for 30 s, annealing at 55 °C for 30 s, and extension at 72 °C for 1 min; with a final extension at 72 °C for 7 min. PCR products were purified and sequenced commercially. Raw sequences were edited and assembled using BioEdit software (version 7.2.5). The obtained ITS sequence was compared with reference sequences in the NCBI GenBank database using BLASTn (Version 2.15.0+, National Center for Biotechnology Information, Bethesda, MD, USA). Multiple sequence alignment was performed using ClustalW (version 2.1) implemented in MEGA X (version 10.2.6). Phylogenetic analysis was conducted using the Maximum Likelihood (ML) method based on the Kimura 2-parameter model. Bootstrap analysis was performed with 1000 replicates to assess branch support. The resulting phylogenetic tree was visualized and exported using MEGA X [20,21].

2.2. Preparation of Heavy Metal Oxides and Culture Conditions

Zinc oxide (ZnO), lead (II, IV) oxide (Pb_3O_4), copper (I) oxide (Cu_2O), and molybdenum trioxide (MoO_3) were used as commercially available analytical-grade bulk powders (non-nanoparticulate). The materials were used as received and were dry-heat sterilized at 160 °C for 2 h prior to incorporation into the medium to minimize contamination. The oxides were supplemented into PDA at a final concentration of 0.5% (w/v), and the medium pH was adjusted to 7.0 before sterilization [22]. Fungal cultivation was initiated using 7 mm diameter mycelial discs placed centrally on the surface of metal-amended PDA plates. Plates were incubated at 25 °C for 7 days [23].

2.3. Evaluation of Fungal Solubilization Potential and Detection of Extracellular Precipitation

All fungal strains were examined for their ability to solubilize the tested heavy metal oxides. After 7 days of incubation, the diameters of clear halo zones surrounding the fungal colonies were measured using three replicate plates. The heavy metal solubilization index (SI) was calculated according to the formula described by Doilom et al. [24] as follows:

$$SI = (\text{Mycelial growth diameter} + \text{Clear zone diameter})/\text{Mycelial growth diameter} \quad (1)$$

The SI was used as a semi-quantitative screening parameter to compare relative dissolution capacity among fungal isolates under standardized culture conditions. The halo boundary was defined as the distinct transparent zone surrounding the fungal colony, where the opacity of the oxide-amended medium was visibly reduced compared to the non-solubilized area. Colony diameter and total diameter (colony plus halo zone) were measured in two perpendicular directions using a digital caliper, and mean values were used for SI calculation. Oxide-amended PDA plates were further incubated for 30 days at room temperature to monitor extracellular precipitation [12]. During incubation, plates were sealed with parafilm to minimize moisture loss and contamination and maintained at room temperature (25 °C). Plates were periodically inspected to ensure no visible contamination or excessive drying occurred. Fungal mycelia and the underlying agar were examined using a stereomicroscope to detect the formation of mycogenic crystals. Strains exhibiting both metal solubilization activity and extracellular crystallization were selected for further investigation of heavy metal biotransformation processes.

2.4. Investigation of Acidification of Selected Fungal Strain

For acidification measurement, the selected fungal strain was grown at pH 7.0 in 250 mL Erlenmeyer flasks with 100 mL potato dextrose broth (PDB) amended with various heavy metal oxides (0.5% *w*/*v*), and PDB without metal oxide supplementation was used as the control. The cultures were incubated in a 125 rpm shaker at 25 °C for 7 days [25]. Each day, aliquots of the culture medium were aseptically collected for pH measurement using a pH meter (Mettler Toledo, 8603, Mettler-Toledo International Inc., Greifensee, Switzerland). All experiments were conducted in triplicate (n = 3), and pH values are presented as mean ± standard deviation.

2.5. Characterization of Extracellular Mycogenic Metal Precipitates

The mycogenic metal crystals were extracted from the PDA plates and put in the test tubes, which were added with 10 mL of double distilled water (ddH_2O). The agar was dissolved by heating in a water bath at 80 °C for 30 min. The mycogenic crystals were left to sink to the bottom of the test tubes and were subsequently filtered to separate the crystals for further analysis [6]. The purified mycogenic crystals were examined for morphology and elemental composition using scanning electron microscopy coupled with energy-dispersive X-ray spectrometry (SEM-EDS; JEOL JSM-IT300, JEOL Ltd, Tokyo, Japan equipped with an Oxford X-Max 20 detector, Oxford Instruments, Oxfordshire, UK). Sample preparation followed the procedures described by Sutjaritvorakul et al. [21] and Gharieb and Gadd [26]. Samples were mounted on aluminum stubs using conductive carbon tape and sputter-coated with a thin layer of gold prior to SEM-EDS analysis to enhance conductivity. Analyses were conducted at an accelerating voltage of 10 kV. Elemental compositions were determined by EDS and expressed as weight percentage (wt.%). Quantification was performed using the instrument's standardless ZAF correction with factory standards. Elemental distribution within the crystal structures was further analyzed by EDS elemental mapping. To confirm the chemical constituents of the crystals, X-ray powder diffraction (XRD) analysis was performed using Cu Kα radiation (λ = 1.5406 Å). The samples were scanned at 40 kV and 50 mA over a 2θ range of 5–90° with a step width of 0.01°. Phase identification was carried out by comparison with reference patterns from the PDF-2 database (International Centre for Diffraction Data, ICDD) [21].

2.6. Statistical Analysis

Statistical analysis of obtained data in triplicate measurements (n = 3) was conducted with GraphPad Prism software 10.0 (GraphPad Software, San Diego, CA, USA). One-way

ANOVA followed by Tukey's test was used to compare the data of the solubilization index with $p \leq 0.05$ as the level of significance.

3. Results

3.1. Investigation of Solubilization Ability and Acidification

Five morphologically distinct fungal isolates were obtained from the mining-contaminated soil and designated as PTW1-PTW5 for preliminary screening of metal solubilization ability. After the incubation period, the clear halo zone can be observed under the fungal colony. The solubilization ability was determined using a solubilization index (SI), which is calculated according to Equation (1), and the results are illustrated in Figure 1. The complete SI values (mean ± SD) for all isolates across tested metal oxides are provided in Supplementary Table S1. The fungal isolate PTW4 showed consistently high solubilization across the tested heavy metal oxides. For zinc oxide (ZnO), the highest SI values were observed in PTW1, PTW2, and PTW4 (2.00), while similarly high values were recorded for lead (II, IV) oxide (Pb_3O_4) in PTW1 and PTW2 (2.00). In the case of copper (I) oxide (Cu_2O), PTW4 showed the highest SI (1.84), followed by PTW1 (1.72), with no significant difference between them. Molybdenum trioxide (MoO_3) generally exhibited lower SI values than the other tested metal oxides, suggesting relatively reduced apparent solubilization under the experimental conditions. PTW4 showed the highest SI for MoO_3 (Figure 1), although this value remained lower than those observed for the other oxides. The solubilization index (SI) provides a comparative, semi-quantitative assessment of dissolution capacity based on halo formation, indicating limited dissolution of MoO_3 under the tested conditions. Overall, PTW4 showed consistently high solubilization performance, whereas PTW5 generally exhibited the lowest SI values. Based on these results, PTW4 was selected for further investigation of its acidification profile. Preliminary morphological observations suggested that PTW4 belonged to the genus Aspergillus, which was later confirmed by molecular identification.

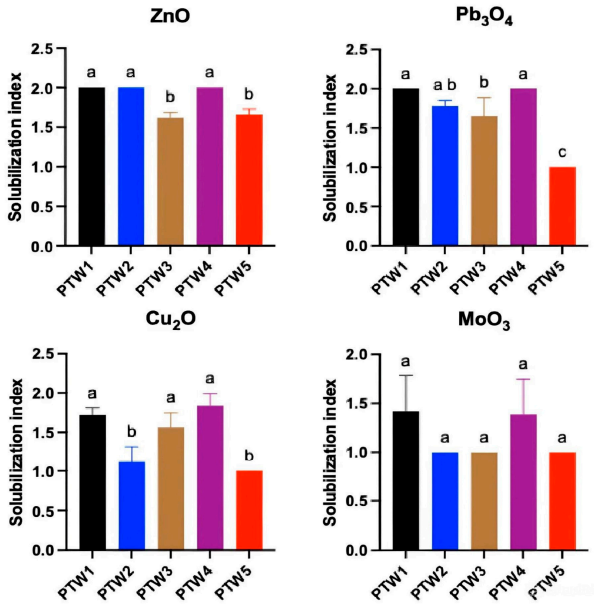


Figure 1. Solubilization index (SI) of fungal isolates grown on agar media containing different heavy metal oxides (0.5% *w*/*v*). Data are presented as mean ± SD ($n = 3$). Different letters indicate statistically significant differences among isolates within each metal oxide treatment ($p < 0.05$).

Figure 2 presents the pH profile of PTW4 during cultivation in PDB supplemented with various heavy metal oxides such as zinc oxide, lead oxide, copper oxide, and molybdenum

trioxide compared with the control (unsupplemented with heavy metal oxides). The pH values were recorded on seven days to investigate the acidification as indicated by the decline in pH. Across all treatments, a progressive decrease in pH was observed, reflecting increased acid production by the fungus over time. The control culture, which contained no heavy metals, showed a gradual decline from pH 7.0 on day 1 to 4.16 on day 7. Cultures supplemented with heavy metal oxides exhibited similar trends, although the rate and magnitude of pH reduction varied among metal types. For instance, zinc oxide supplementation resulted in a drop from pH 7.0 on day 1 to 4.28 on day 7, while copper oxide led to a reduction from pH 7.0 to 4.31 over the same period. Lead oxide and molybdenum trioxide treatments also demonstrated sustained decreases, reaching pH 4.56 and 5.42, respectively, by day 7. Overall, the data indicate that the fungus continued to produce organic acids under all conditions, with heavy metal presence influencing but not preventing acidification of the medium.

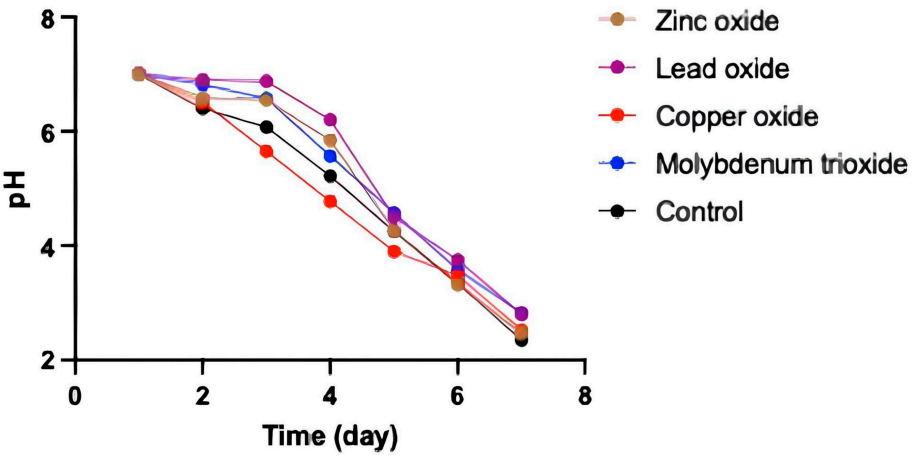


Figure 2. Temporal pH profiles of PDB during cultivation of the selected fungal strain PTW4 in the presence of various heavy metal oxides (0.5% *w*/*v*). The control represents PDB without metal supplementation. Values are expressed as mean ± SD (n = 3).

3.2. Characterization and Chemical Analysis of Extracellular Mycogenic Metal Precipitates

All oxide-amended PDA plates were incubated for 30 days. The extracellular precipitates were found beneath the colonies of the fungal strain PTW4. Crystal formation was first visually observed after approximately 21 days of incubation and progressively increased during the incubation period. No visible mineral precipitates were observed in control plates without metal oxide supplementation. After purification, these crystal precipitates were then investigated for morphological characterization and chemical analysis. SEM investigation revealed distinct morphological characteristics of mycogenic precipitates. Figure 3 exhibits morphological characteristics of mycogenic precipitates produced by strain PTW4 when grown on PDA supplemented with different metal oxides. In ZnO-amended medium, the fungus generated compact, oval-shaped precipitates (Figure 3A), as well as clusters of layered structures located beneath the fungal colony (Figure 3B). In the presence of Pb_3O_4, PTW4 formed irregular and dense aggregates of precipitates (Figure 3C). At high magnification (×1000) imaging showed that these lead associated minerals accumulated directly on the fungal mycelium (arrows) (Figure 3D), indicating hyphal involvement in the nucleation and deposition of lead containing crystals. The crystal precipitates produced in Cu_2O supplemented medium exhibited distinct lamellar or layered morphologies (Figure 3E). These biominerals were frequently observed adhering to and surrounding the fungal hyphae (Figure 3F), demonstrating that the mycelium serves as an active surface for copper mineral attachment and transformation.

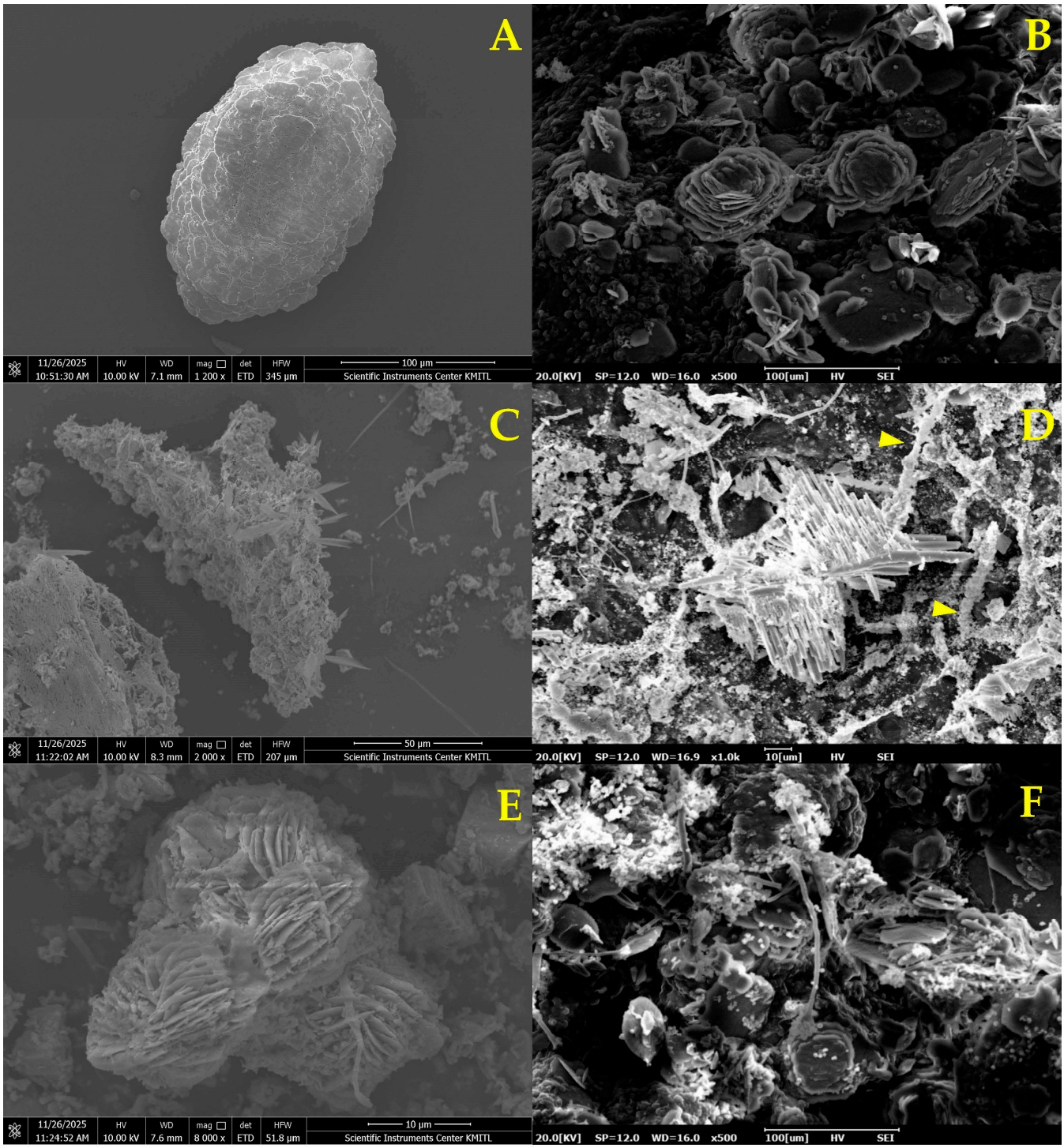


Figure 3. SEM micrograph of extracellular mycogenic precipitates generated by selected fungal strain PTW4. (**A**) Mycogenic precipitates formed in PDA supplemented with ZnO, Scale bar = 100 µm. (**B**) The group of precipitates under the fungal colony, Scale bar = 100 µm. (**C**) Mycogenic precipitates formed in PDA supplemented with Pb_3O_4, Scale bar = 50 µm. (**D**) Mycogenic precipitates associated, and accumulated on the fungal mycelium (arrows), Scale bar = 10 µm. (**E**) Mycogenic precipitates formed in PDA supplemented with Cu_2O, Scale bar = 10 µm. (**F**) Mycogenic precipitates associated with the fungal mycelium, Scale bar = 100 µm.

For elemental analysis, energy-dispersive X-ray spectroscopy (EDS) coupled with elemental mapping was performed to verify the elemental composition of the mycogenic precipitates generated by fungal strain PTW4 in metal-amended media (Figure 4). The

precipitates obtained from ZnO supplemented medium showed strong characteristic carbon, oxygen, and zinc peaks in the EDS spectrum (Figure 4A) at 57.91 wt%, 31.29%, and 10.79%, respectively, and the corresponding elemental map confirmed that zinc (red), carbon (green), and oxygen (yellow) were uniformly distributed across the precipitate structure. For precipitates formed in Pb_3O_4 supplemented medium, the EDS spectrum revealed strong peak of lead (Figure 4B). Quantitative analysis showed that the precipitates were primarily composed of three major elements such as carbon (56.83%), oxygen (31.59%), and lead (11.59%). Elemental mapping further demonstrated dense accumulation of lead (orange), carbon (green), and oxygen (yellow) throughout the metal precipitates. Similarly, precipitates originating from Cu_2O-amended medium displayed distinct copper peaks in the EDS spectrum (Figure 4C). The elemental composition consisted mainly of carbon (37.22%), oxygen (37.71%), and copper (25.07%). The corresponding elemental map showed copper rich regions (cyan) concentrated within the layered structures of the precipitate, with carbon (green), and oxygen (yellow) distributed throughout the crystal precipitates.

Chemical composition and identification of crystal precipitates, Figure 5 shows X-ray powder diffraction analysis. Figure 5A displays diffraction peaks that closely matched those of zinc oxalate dihydrate ($ZnC_2O_4 \cdot 2H_2O$), corresponding to PDF card No. 00-025-1029, confirming that the fungal mediated transformation resulted in the formation of crystalline zinc oxalate. Correspondingly, the precipitates obtained from Pb_3O_4 supplemented medium showed diffraction signals characteristic of lead oxalate (PbC_2O_4), corresponding to PDF card No. 00-014-0803 (Figure 5B). The alignment of peak positions between the sample profile and the reference pattern indicates that the fungus facilitated the bioprecipitation of crystalline lead oxalate. For mycogenic precipitates from Cu_2O-amended medium, the XRD pattern of the resulting precipitate (Figure 5C) showed an excellent match to standard diffraction pattern of copper oxalate hydrate ($CuC_2O_4 \cdot xH_2O$), also known as moolooite (corresponding to PDF card No. 00-021-0297). The distinct and intense peaks shared with the reference standard confirm copper oxalate as the dominant mineral phase generated through fungal activity. These results collectively indicate that fungal strain PTW4 effectively mediates the deposition and transformation of zinc oxide, lead oxide, and copper oxide into their corresponding oxalate mineral forms via mycogenic biomineralization, which represent insoluble mineral phases with substantially reduced ecological toxicity.

3.3. Molecular Identification of Selected Fungal Strain PTW4

Approximately 492 bp of ITS rDNA sequence data were obtained from fungal strain PTW4 and compared with sequences available in the NCBI GenBank database using BLASTn. The analysis showed 100% sequence similarity to reference sequences of *Aspergillus aculeatus*, indicating that strain PTW4 is closely related to this species. Identification was based on ITS sequence similarity to reference sequences available in GenBank (NR_111412.1); however, the ITS sequence of strain PTW4 has not yet been deposited in a public database. To further support the identification and illustrate phylogenetic placement, an ITS-based phylogenetic tree was constructed using reference sequences from closely related *Aspergillus* species (Figure 6). The phylogenetic analysis showed that strain PTW4 clustered within the *A. aculeatus* clade with high bootstrap support, consistent with the BLAST results. An outgroup sequence from a closely related *Aspergillus* lineage outside the *A. aculeatus* clade was included to provide rooting and evolutionary context for the phylogenetic analysis. However, ITS sequences alone may be insufficient to resolve strain-level differences, and additional loci such as BenA or CaM could improve taxonomic resolution.

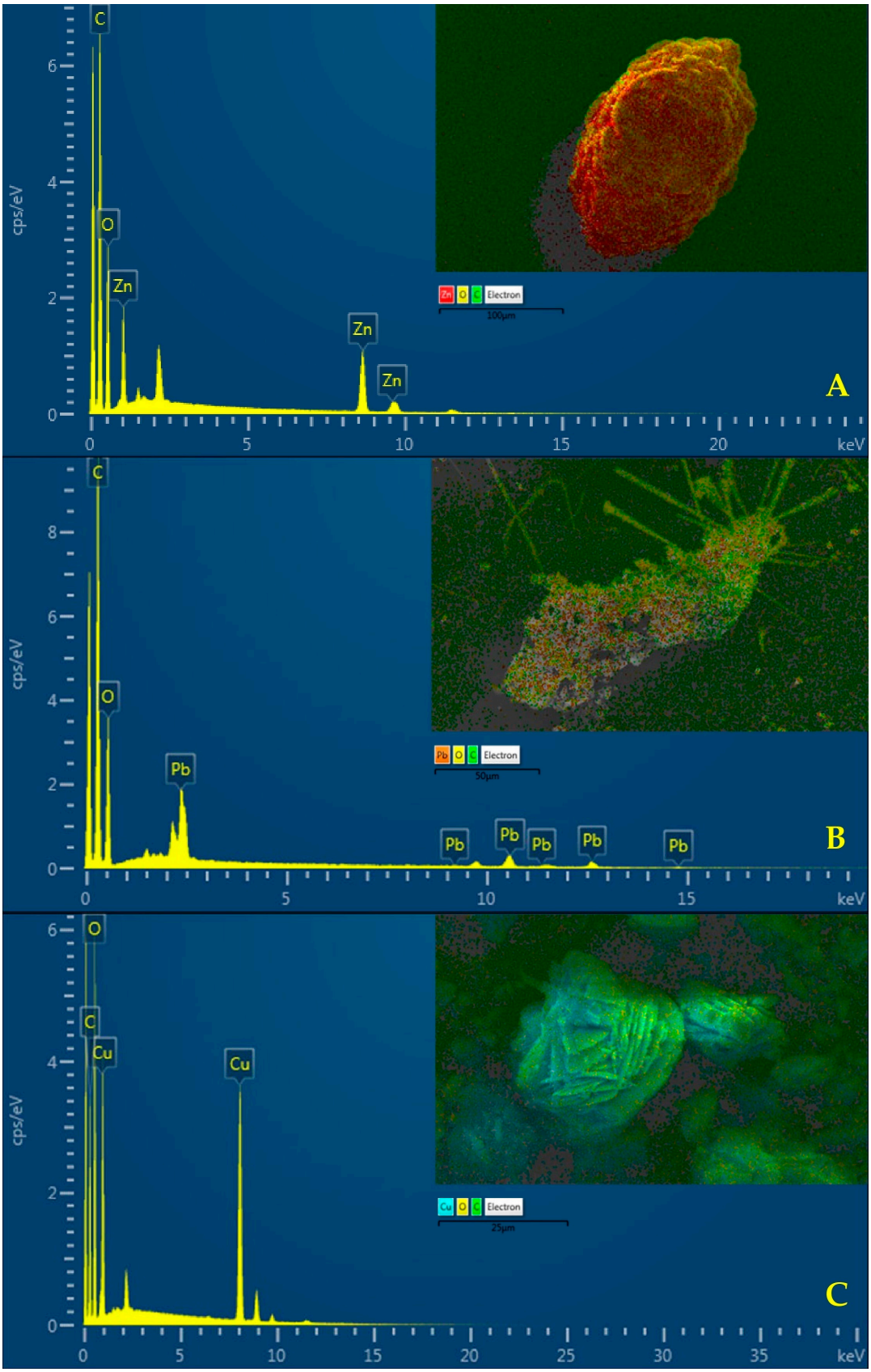


Figure 4. EDS spectra and elemental mapping of mycogenic precipitates produced by selected fungal isolate (PTW4). (**A**) Purified precipitates formed on ZnO supplemented medium, Scale bar = 100 µm. (**B**) Purified precipitates formed on Pb_3O_4 supplemented medium, Scale bar = 50 µm. (**C**) Purified precipitates formed on Cu_2O supplemented medium, Scale bar = 25 µm.

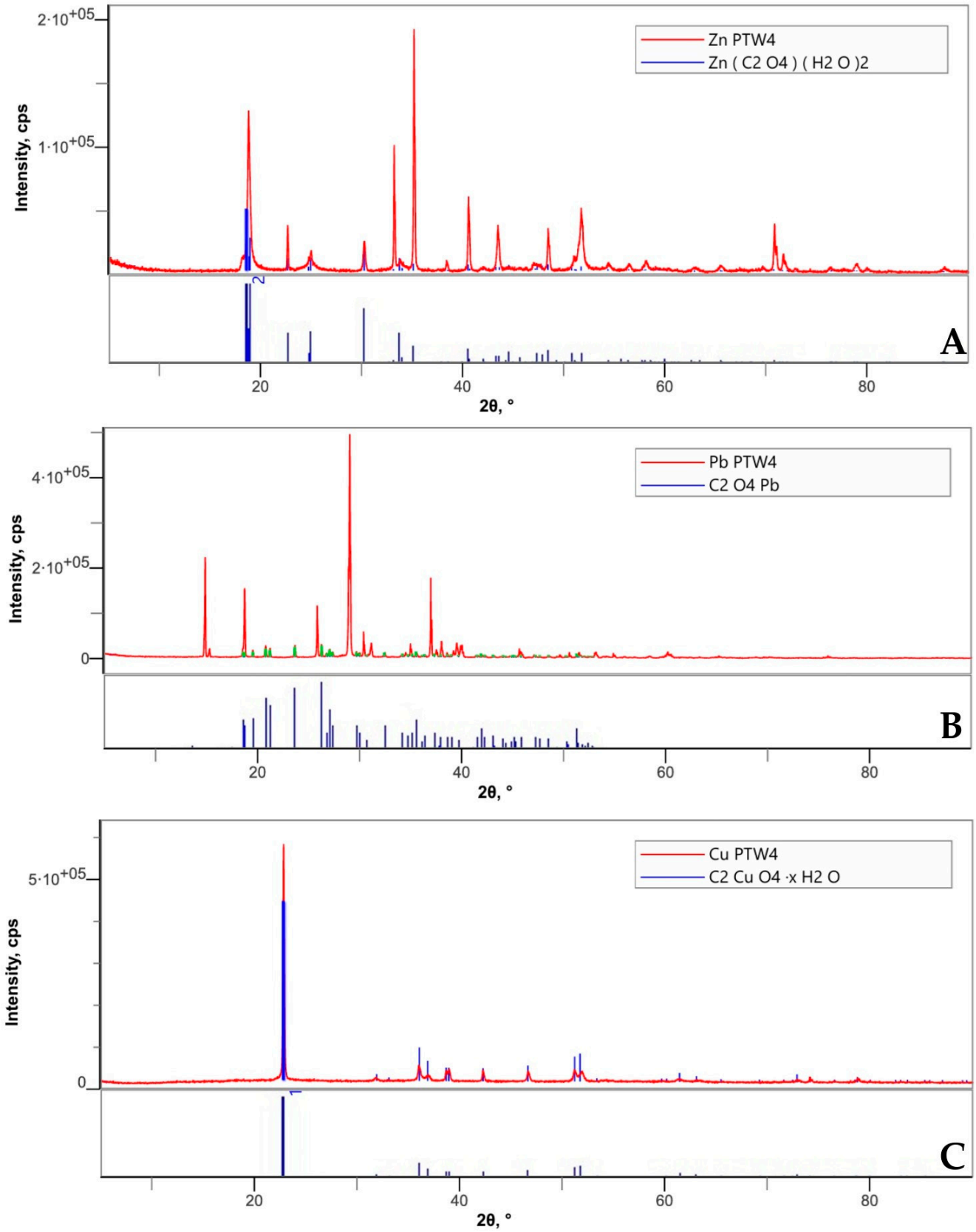


Figure 5. X-ray powder diffraction profiles of mycogenic precipitates produced by fungal strain PTW4. (**A**) Diffraction profile of zinc oxalate, (**B**) Diffraction profile of lead oxalate, and (**C**) Diffraction profile of copper oxalate. The green line represents the reference pattern used for phase identification.

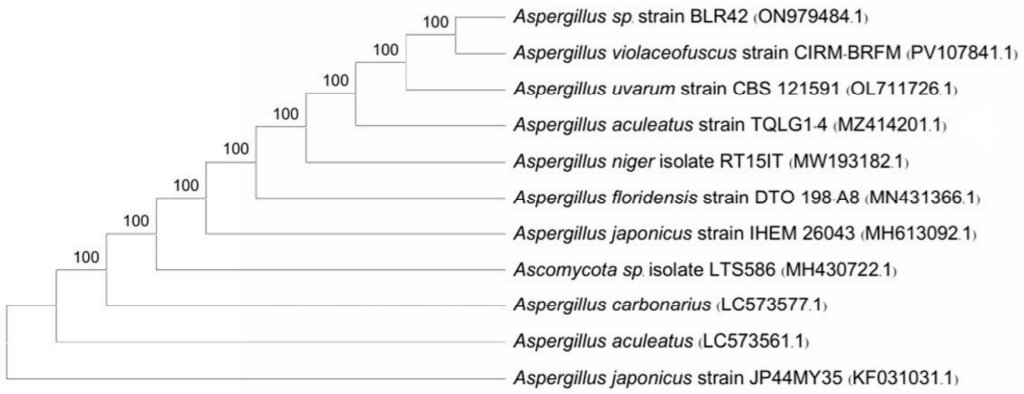


Figure 6. ITS-based phylogenetic tree showing the relationship between fungal isolate PTW4 and reference *Aspergillus aculeatus* sequences. The tree supports the BLAST-based species identification.

4. Discussion

Soil fungi are recognized as important contributors to biogeochemical processes influencing metal mobility and mineral transformation in terrestrial environments [27,28]. The genus *Aspergillus* is commonly found in soil, including heavy metal-polluted soil [29,30]. Fungi in this group are tolerant of and adaptable to metal-contaminated environments, exhibiting diverse biochemical and physiological responses [31]. They often generate free organic acids that are directly involved in the metal solubilization process, resulting in a decrease in system pH during growth [27]. One of the key factors influencing metal solubilization is pH value of the system, especially in the low pH value. The acidification increases the solubility of metal compounds [28]. The pH profile (Figure 2) showed a decrease in pH values for both the heavy metal oxide supplemented medium and the control, suggesting that acidification was primarily driven by fungal physiological processes rather than being induced by the presence of metal oxides. Filamentous soil fungi in the *Aspergillus* and *Penicillium* groups have a high potential to generate proton efflux (H^+) and free organic acids via the respiration process, which facilitate metal solubilization in the environment. Moreover, the free organic acid produced by *Aspergillus* spp. such as citric and oxalic acid, play a major role in metal precipitation through the formation of metal oxalate complex [32–34]. Heavy metal oxide supplementation moderately influenced the rate of pH change; however, it did not suppress acid production. This indicates that PTW4 possibly employs proton efflux and organic acid release as its principal solubilization strategy, consistent with the documented role of oxalate secretion in fungal weathering processes. This study was designed as an initial screening investigation to identify fungal isolates with metal solubilization potential. While the solubilization index provides a useful comparative indicator of dissolution capacity, quantitative determination of dissolved metals (e.g., ICP-based analysis) would be required for a more precise evaluation of metal mobilization dynamics and should be addressed in future studies. Furthermore, oxalic acid not only enhances metal dissolution but also facilitates the formation of secondary biominerals such as metal oxalates, a mechanism widely recognized in fungal biomineralization [27,33]. These processes provide a plausible explanation for the precipitation patterns observed in the SEM-EDS and XRD analyses.

SEM-EDS analyses demonstrated element-specific enrichment in these structures, and XRD indicated crystalline phases consistent with metal oxalates ($ZnC_2O_4{\cdot}2H_2O$, PbC_2O_4, and $CuC_2O_4{\cdot}xH_2O$). These complementary observations are consistent with well-documented fungal biomineralization pathways in which extracellular oxalate is frequently implicated in metal immobilization and mineral precipitation [35]. Mechanistically, fungi commonly excrete oxalic acid and other organic acids that chelate dissolved metal ions and lower local pH, promoting supersaturation and subsequent precipitation of insoluble metal–

oxalate phases. The high carbon and oxygen contents detected by EDS (e.g., C (56.8%) and O (31.6%) in Pb precipitates; C (37.2%) and O (37.7%) in Cu precipitates) (Figure 4) support an organic–mineral composite composition consistent with oxalate-associated phases together with the target metals. Oxalic acid-driven formation of Zn, Pb, and Cu oxalates by fungi has been reported in multiple studies and is regarded as a common strategy for detoxification, metal sequestration, and mineral formation [35,36]. Mycogenic crystals forming directly on hyphae or in hyphal aggregates indicate that the fungal cell surface and extracellular polymeric substances (EPS) may serve as nucleation templates. Organic functional groups on the cell wall (carboxyl, hydroxyl, phosphate) can locally concentrate metal ions and provide nucleation sites, producing the characteristic morphologies. Similar hypha-associated nucleation and layered morphologies have been documented for fungal precipitation of zinc and copper oxalates in previous studies [23,37]. Differences among the three metals in crystal morphology, element proportions, and XRD peak intensities likely reflect metal-specific chemistry (solubility, complexation constants with oxalate), ion availability in the microenvironment, and kinetics of nucleation and growth. For instance, the relatively lower atomic percentage of Pb (11.6%) in the Pb-derived precipitates (EDS), despite strong Pb XRD peaks, may reflect a substantial organic fraction in the analyzed particles or hydration/structural water in the crystal lattice; this is consistent with reports that fungal oxalate precipitates commonly contain large organic fractions and variable hydration states that influence EDS bulk percentages and XRD intensities [38,39]. Although oxalate production was not directly quantified in this study, the identification of oxalate-associated mineral phases by XRD supports a plausible oxalate-mediated biomineralization mechanism. The high carbon content detected by EDS may reflect contributions from oxalate-containing mineral phases together with residual organic matrices and possible background signals associated with sample preparation, such as carbon tape. These factors should be considered when interpreting elemental compositions, as EDS provides semi-quantitative surface information rather than definitive stoichiometric determination. In addition, the extraction procedure was conducted at 80 °C following established protocols [6]. Although moderate heating could potentially influence the hydration states of certain mineral phases, no evidence of secondary phase transformation or recrystallization was observed in the XRD patterns obtained in this study. The absence of molybdenum precipitation observed in this study further highlights metal-specific constraints in fungal biomineralization processes. Although effective solubilization of MoO_3 was observed, molybdenum remained predominantly in the aqueous phase under the tested conditions, indicating limited propensity for oxalate-mediated immobilization. Under mildly acidic to near-neutral conditions (approximately pH 4–6), dissolved molybdenum is predominantly present as molybdate species (e.g., MoO_4^{2-}), which are highly soluble and less likely to form stable precipitates with oxalate compared with divalent metal cations such as Zn^{2+}, Pb^{2+}, and Cu^{2+}. Consequently, oxalate-mediated precipitation of molybdenum may be thermodynamically unfavorable under the tested conditions. This behavior is consistent with the aqueous chemistry of molybdenum and with our previous findings using wood-decaying fungi, in which MoO_3 was readily solubilized but no stable molybdenum biominerals were detected despite active fungal growth and acidification [40]. Collectively, these observations suggest that, unlike Zn, Pb, and Cu, molybdenum exhibits distinct geochemical behavior that constrains its precipitation as fungal-derived oxalate minerals. It should be noted that the oxide concentration and nutrient-rich culture conditions applied in this study were designed for preliminary laboratory screening and may not fully represent natural soil environments. Therefore, further validation under soil-based or microcosm conditions would be necessary to assess environmental applicability.

The molecular identification confirmed that strain PTW4 belongs to *Aspergillus aculeatus*. The present study demonstrated that *A. aculeatus* strain PTW4 exhibits a strong ability to solubilize various heavy metal oxides, accompanied by progressive acidification of the culture medium. Members of the genus *Aspergillus* are widely recognized for their roles in metal weathering, organic acid production, and biomineral transformations in soil ecosystems [27,41]. However, reports describing the involvement of *A. aculeatus* specifically in heavy metal solubilization or biotransformation remain extremely limited. Most studies have focused on species such as *Aspergillus niger* and *Aspergillus terreus*, which are well known for secreting high levels of citric and oxalic acids [32,33]. In this research, the performance of strain PTW4 is notable because it expands the range of *Aspergillus* species associated with metal mobilization. PTW4 produced substantial acidification regardless of metal type, indicating that the presence of heavy metal oxides did not inhibit organic acid secretion. This observation aligns with the general resilience and metabolic flexibility of *Aspergillus* spp. in metal-rich environments [29,31]. Although studies directly addressing the metal transformation ability of *A. aculeatus* are very few, several reports have documented its secretion of organic acids, including citric, tartaric, gluconic, and aminoacetic acid, in agricultural contexts as a phosphate-solubilizing fungus. Not only do organic acids play a role, but this fungus also secretes the enzyme phosphatase, which collaborates with organic acids to effectively solubilize a rock phosphate [42,43]. To the best of our knowledge, this study provides one of the first experimental characterizations of heavy metal-solubilizing behavior in *A. aculeatus*, particularly across multiple heavy metal oxide compounds. The findings therefore expand current understanding of the functional diversity of *Aspergillus* spp. in metal cycling and highlight *A. aculeatus* PTW4 as a relevant model for further investigations into fungal biomineralization and exploratory bioremediation studies.

5. Conclusions

Aspergillus aculeatus (PTW4), isolated from mining-contaminated soil, was able to solubilize all tested heavy metal oxides, including Zn, Pb, Cu, and Mo. Extracellular biomineralization occurred selectively with Zn, Pb, and Cu, resulting in poorly soluble metal oxalate phases, whereas molybdenum remained in solution, indicating metal-specific constraints in fungal biomineralization pathways. Although oxalate production was not directly quantified, identification of crystalline oxalate-associated phases by XRD supports a plausible oxalate-mediated precipitation mechanism. These mineral phases may reduce metal mobility under the tested conditions, highlighting the ecological relevance of fungal-mediated metal transformation. Because this study was conducted under controlled laboratory conditions using nutrient-rich media, further validation in soil microcosm and environmentally relevant systems is required before practical bioremediation or selective bioleaching applications can be assessed. Future work should focus on direct quantification of organic acids, clarification of metabolic mechanisms governing metal specificity, and evaluation of process performance under more complex environmental conditions.

Supplementary Materials: The following supporting information can be downloaded at: https://www.mdpi.com/article/10.3390/jox16020044/s1, Table S1: Solubilization index (SI) values of fungal isolates for each tested metal oxide (mean ± SD, n = 3).; Figure S1: Original uncropped SEM image corresponding to Figure 3A; Figure S2: Original uncropped SEM image corresponding to Figure 3B; Figure S3: Original uncropped SEM image corresponding to Figure 3C; Figure S4: Original uncropped SEM image corresponding to Figure 3D; Figure S5: Original uncropped SEM image corresponding to Figure 3E; Figure S6: Original uncropped SEM image corresponding to Figure 3F; Figure S7: Original uncropped SEM image corresponding to Figure 4A; Figure S8: Original uncropped SEM image corresponding to Figure 4B; Figure S9: Original uncropped SEM image corresponding to Figure 4C.

Author Contributions: Conceptualization, T.S. (Thanawat Sutjaritvorakul); methodology, T.S. (Thanawat Sutjaritvorakul) and T.S. (Thanakorn Sawangchart); validation, T.S. (Thanakorn Sawangchart), B.M. and T.S. (Thanawat Sutjaritvorakul); formal analysis, T.S. (Thanakorn Sawangchart); investigation, T.S. (Thanakorn Sawangchart), P.I., W.N. and W.T.; resources, S.C.; data curation, T.S. (Thanawat Sutjaritvorakul); writing—original draft preparation, T.S. (Thanawat Sutjaritvorakul) and T.S. (Thanakorn Sawangchart); writing—review and editing, T.S. (Thanawat Sutjaritvorakul), B.M.; visualization, T.S. (Thanawat Sutjaritvorakul); supervision, T.S. (Thanawat Sutjaritvorakul); project administration, T.S. (Thanawat Sutjaritvorakul); funding acquisition, S.C. All authors have read and agreed to the published version of the manuscript.

Funding: This research was funded by King Mongkut's Institute of Technology Ladkrabang research fund, grant number KREF046803.

Institutional Review Board Statement: Not applicable.

Informed Consent Statement: Not applicable.

Data Availability Statement: The original contributions presented in this study are included in the article/Supplementary Materials. Further inquiries can be directed to the corresponding author.

Conflicts of Interest: The authors declare no conflicts of interest.

Abbreviations

The following abbreviations are used in this manuscript:

SI	Solubilization Index
PDA	Potato Dextrose Agar
PDB	Potato Dextrose Broth
SEM	Scanning Electron Microscope
EDS	Energy Dispersive Spectroscope
XRD	X-ray Diffraction
ddH_2O	double distilled water

References

1. Razzak, S.A.; Faruque, M.O.; Alsheikh, Z.; Alsheikhmohamad, L.; Alkuroud, D.; Alfayez, A.; Hossain, S.M.Z.; Hossain, M.M. A comprehensive review on conventional and biological-driven heavy metals removal from industrial wastewater. *Environ. Adv.* **2022**, *7*, 100168. [CrossRef]
2. Scutarașu, E.C.; Trincă, L.C. Heavy metals in foods and beverages: Global situation, health risks and reduction methods. *Foods* **2023**, *12*, 3340. [CrossRef] [PubMed]
3. Gakis, G.P.; Aviziotis, I.G.; Charitidis, C.A. Metal and metal oxide nanoparticle toxicity: Moving towards a more holistic structure–activity approach. *Environ. Sci. Nano* **2023**, *10*, 761–780. [CrossRef]
4. Kolya, H.; Kang, C.W. Toxicity of metal oxides, dyes, and dissolved organic matter in water: Implications for the environment and human health. *Toxics* **2024**, *12*, 111. [CrossRef]
5. Hamdan, A.M.; Abd-El-Mageed, H.; Ghanem, N. Biological treatment of hazardous heavy metals by *Streptomyces rochei* ANH for sustainable water management in agriculture. *Sci. Rep.* **2021**, *11*, 9314. [CrossRef]
6. Kaewdoung, B.; Sutjaritvorakul, T.; Gadd, G.M.; Whalley, A.J.S.; Sihanonth, P. Heavy metal tolerance and biotransformation of toxic metal compounds by new isolates of wood-rotting fungi from Thailand. *Geomicrobiol. J.* **2016**, *33*, 283–288. [CrossRef]
7. Kondakindi, V.R.; Pabbati, R.; Erukulla, P.; Maddela, N.R.; Prasad, R. Bioremediation of heavy metals-contaminated sites by microbial extracellular polymeric substances: A critical view. *J. Environ. Chem. Ecotoxicol.* **2024**, *6*, 408–421. [CrossRef]
8. Kolo, K.; Préat, A. In vitro experimental observations on fungal colonization, metalophagus behavior, tunneling, bioleaching and bioweathering of multiple mineral substrates. *Minerals* **2023**, *13*, 1540. [CrossRef]
9. Gadd, G.M. Interactions of fungi with toxic metals. *New Phytol.* **1993**, *124*, 25–60. [CrossRef]
10. Amobonye, A.; Aruwa, C.E.; Aransiola, S.; Omame, J.; Alabi, T.D.; Lalung, J. The potential of fungi in the bioremediation of pharmaceutically active compounds: A comprehensive review. *Front. Microbiol.* **2023**, *14*, 1207792. [CrossRef]
11. Gadd, G.M. Mycotransformation of organic and inorganic substrates. *Mycologist* **2004**, *18*, 60–69. [CrossRef]
12. Fomina, M.; Hillier, S.; Charnock, J.M.; Melville, K.; Alexander, I.J.; Gadd, G.M. Role of oxalic acid overexcretion in transformations of toxic metal minerals by *Beauveria caledonica*. *Appl. Environ. Microbiol.* **2005**, *71*, 371–381. [CrossRef]

13. Iram, S.; Zaman, A.; Iqbal, Z.; Shabbir, R. Heavy metal tolerance of fungus isolated from soil contaminated with sewage and industrial wastewater. *Pol. J. Environ. Stud.* **2013**, *22*, 691–697.
14. Oladipo, O.G.; Awotoye, O.O.; Olayinka, A.; Bezuidenhout, C.C.; Maboeta, M.S. Heavy metal tolerance traits of filamentous fungi isolated from gold and gemstone mining sites. *Braz. J. Microbiol.* **2018**, *49*, 29–37. [CrossRef]
15. Arellano, J.A.E.; Argame, I.B.M.; Castillo, F.R.G.; Salazar, C.G.E.; Lopez, M.K.S. Evaluation of tolerance and uptake of Cd and Mn by microfungi *Aspergillus flavus*, *Aspergillus oryzae*, and *Aspergillus terreus* isolated from landfill soil collected from Bangar, La Union, Philippines. *Environ. Nat. Resour. J.* **2024**, *22*, 184–196. [CrossRef]
16. Ramos Suárez, D.E.; Valdivia-Flores, A.G.; Guerrero Barrera, A.L.; Flores Amaro, O.A.; Yamamoto Flores, L.; Gutierrez Corona, J.F.; Bautista Bautista, J.C.; Avelar González, F.J. Cadmium and lead tolerance of filamentous fungi isolated from contaminated mining soils. *Biology* **2025**, *16 14*, 688. [CrossRef]
17. Li, X.; Ren, X.; Chen, H.; Xin, Y.; Zhou, T.; Yan, J.; Xu, J.; Ijaz, M.; Ahmed, T.; Li, B.; et al. Isolation of multiple plant growth-promoting fungi and their effect on rice growth improvement on non-grain converted land. *Front. Plant Sci.* **2025**, *16*, 1618073. [CrossRef]
18. Olumuyiwa, E.O.; Ajetunmobi, M.T.; Adeniji, O.F.; Ogunyemi, A.K. Morphological and molecular identification of fungi isolated from spoilt apples in Ota metropolis. *BMC Microbiol.* **2025**, *25*, 360. [CrossRef] [PubMed]
19. Barnett, H.L.; Hunter, B.B. *Illustrated Genera of Imperfect Fungi*, 4th ed.; APS Press: St. Paul, MN, USA, 1998; p. 218.
20. Moropana, T.J.; Jansen Van Rensburg, E.L.; Makulana, L.; Phasha, N.N. Screening *Aspergillus flavus*, *Talaromyces purpureogenus*, and *Trichoderma koningiopsis* for plant-growth-promoting traits: A study on phosphate solubilization, IAA production, and siderophore synthesis. *J. Fungi* **2024**, *10*, 811. [CrossRef]
21. Sutjaritvorakul, T.; Gadd, G.M.; Whalley, A.J.S.; Suntornvongsagul, K.; Sihanonth, P. Zinc oxalate crystal formation by *Aspergillus nomius*. *Geomicrobiol. J.* **2016**, *33*, 289–293. [CrossRef]
22. Sayer, J.A.; Raggett, S.L.; Gadd, G.M. Solubilization of insoluble metal compounds by soil fungi: Development of a screening method for solubilizing ability and metal tolerance. *Mycol. Res.* **1995**, *99*, 987–993. [CrossRef]
23. Sutjaritvorakul, T.; Gadd, G.M.; Suntornvongsagul, K.; Whalley, A.J.S.; Roengsumran, S.; Sihanonth, P. Solubilization and Transformation of Insoluble Zinc Compounds by Fungi Isolated from a Zinc Mine. *Environ. Asia* **2013**, *6*, 42–46.
24. Doilom, M.; Guo, J.-W.; Phookamsak, R.; Mortimer, P.E.; Karunarathna, S.C.; Dong, W.; Liao, C.-F.; Yan, K.; Pem, D.; Suwannarach, N.; et al. Screening of phosphate-solubilizing fungi from air and soil in Yunnan, China: Four novel species in *Aspergillus*, *Gongronella*, *Penicillium*, and *Talaromyces*. *Front. Microbiol.* **2020**, *11*, 585215. [CrossRef]
25. Li, Q.; Zhang, M.; Wei, B.; Lan, W.; Wang, Q.; Chen, C.; Zhao, H.; Liu, D.; Gadd, G.M. Fungal biomineralization of toxic metals accelerates organic pollutant removal. *Curr. Biol.* **2024**, *34*, 2077–2084. [CrossRef]
26. Gharieb, M.M.; Gadd, G.M. Influence of nitrogen source on the solubilization of natural gypsum ($CaSO_4 \cdot 2H_2O$) and the formation of calcium oxalate by different oxalic and citric acid-producing fungi. *Mycol. Res.* **1999**, *103*, 473–481. [CrossRef]
27. Gadd, G.M. Minerals and microbes: Geomicrobiology and bioremediation. *Microbiology* **2010**, *156*, 609–643. [CrossRef]
28. Tian, D.; Zhang, S.; Wang, D.; Zhang, L.; Chen, H.; Ye, X. Heavy metal remediation using phosphate-solubilizing fungi: From bioprocess to application. *Agronomy* **2024**, *14*, 2638. [CrossRef]
29. Castro-Ríos, K.; Buri, M.C.S.; Ramalho da Cruz, A.D.; Ceresini, P.C. *Aspergillus fumigatus* in the food production chain and azole resistance: A growing concern for consumers. *J. Fungi* **2025**, *11*, 252. [CrossRef]
30. Rabab, A.; Asmaa, S.; Asmaa, H.; Shereen, A. Adaptability assessment of *Aspergillus niger* and *Aspergillus terreus* isolated from long-term municipal/industrial effluent-irrigated soils to cadmium stress. *BMC Microbiol.* **2025**, *25*, 297. [CrossRef] [PubMed]
31. Robinson, J.R.; Isikhuemhen, O.S.; Anike, F.N. Fungal–metal interactions: A review of toxicity and homeostasis. *J. Fungi* **2021**, *7*, 225. [CrossRef] [PubMed]
32. Burgstaller, W.; Schinner, F. Leaching of metals with fungi. *J. Biotechnol.* **1993**, *27*, 91–116. [CrossRef]
33. Sayer, J.A.; Gadd, G.M. Solubilization and transformation of insoluble metal compounds by fungi. *Mycologist* **1997**, *11*, 98–104. [CrossRef]
34. Alemayehu, K.; Jiru, T.M.; Berhane, N. Diversity of organic acid-producing filamentous fungi isolated from agricultural soils of North Gondar, Ethiopia. *Scientifica* **2025**, *2025*, 9186819. [CrossRef] [PubMed]
35. Gadd, G.M.; Bahri-Esfahani, J.; Li, Q.; Rhee, Y.J.; Wei, Z.; Fomina, M.; Liang, X. Oxalate production by fungi: Significance in geomycology, biodeterioration and bioremediation. *Fungal Biol. Rev.* **2014**, *28*, 36–55. [CrossRef]
36. Grąz, M. Role of oxalic acid in fungal and bacterial metabolism and its biotechnological potential. *World J. Microbiol. Biotechnol.* **2024**, *40*, 178. [CrossRef]
37. Wei, Z.; Liang, X.; Pendlowski, H.; Hillier, S.; Suntornvongsagul, K.; Sihanonth, P.; Gadd, G.M. Fungal biotransformation of zinc silicate and sulfide mineral ores. *Environ. Microbiol.* **2013**, *15*, 2173–2186. [CrossRef]
38. Kornyakov, I.V.; Gurzhiy, V.V.; Kuz'mina, M.A.; Krzhizhanovskaya, M.G.; Chukanov, N.V.; Chislov, M.V.; Korneev, A.V.; Izatulina, A.R. Crystal chemistry of the copper oxalate biomineral moolooite: The first single-crystal X-ray diffraction studies and thermal behavior. *Int. J. Mol. Sci.* **2023**, *24*, 6786. [CrossRef]

39. Vlasov, D.Y.; Zelenskaya, M.S.; Izatulina, A.R.; Janson, S.Y.; Frank-Kamenetskaya, O.V. Oxalate crystallization under the action of brown rot fungi. *Crystals* **2023**, *13*, 432. [CrossRef]
40. Sutjaritvorakul, T.; Chutipaijit, S. Solubilization and tolerance of molybdenum trioxide (MoO_3) by wood decaying fungi. *Khon Kaen Agr. J.* **2017**, *45*, 179–188.
41. Gadd, G.M. Fungal biomineralization. *Curr. Biol.* **2021**, *31*, R1557–R1563. [CrossRef]
42. Narsian, V.; Patel, H.H. *Aspergillus aculeatus* as a rock phosphate solubilizer. *Soil Biol. Biochem.* **2000**, *32*, 559–562. [CrossRef]
43. Li, X.; Sun, X.; Wang, G.; Amombo, E.; Zhou, X.; Du, Z.; Zhang, Y.; Xie, Y.; Fu, J. Inoculation with *Aspergillus aculeatus* alters the performance of perennial ryegrass under phosphorus deficiency. *J. Am. Soc. Hortic. Sci.* **2019**, *144*, 182–192. [CrossRef]

Disclaimer/Publisher's Note: The statements, opinions and data contained in all publications are solely those of the individual author(s) and contributor(s) and not of MDPI and/or the editor(s). MDPI and/or the editor(s) disclaim responsibility for any injury to people or property resulting from any ideas, methods, instructions or products referred to in the content.